Family of Ideal Chern Flatbands with Arbitrary Chern Number in Chiral Twisted Graphene Multilayers

Patrick J. Ledwith, Ashvin Vishwanath, and Eslam Khalaf

A family of ideal Chern flat bands with arbitrary Chern number in chiral twisted graphene multilayers

Patrick J. Ledwith, Ashvin Vishwanath, Eslam Khalaf

Department of Physics, Harvard University, Cambridge, MA 02138

We consider a family of twisted graphene multilayers consisting of n-untwisted chirally stacked layers, e.g. AB, ABC, etc, with a single twist on top of m-untwisted chirally stacked layers. Upon neglecting both trigonal warping terms for the untwisted layers and the same sublattice hopping between all layers, the resulting models generalize several remarkable features of the chiral model of twisted bilayer graphene (CTBG). In particular, they exhibit a set of magic angles which are identical to those of CTBG at which a pair of bands (i) are perfectly flat, (ii) have Chern numbers in the sublattice basis given by $\pm(n, -m)$ or $\pm(n + m - 1, -1)$ depending on the stacking chirality, and (iii) satisfy the trace condition, saturating an inequality between the quantum metric and the Berry curvature, and thus realizing ideal quantum geometry. These are the first higher Chern bands that satisfy (iii) beyond fine-tuned models or combinations of Landau levels. We show that ideal quantum geometry is directly related to the construction of fractional quantum Hall model wavefunctions. We provide explicit analytic expressions for the flat band wavefunctions at the magic angle in terms of the CTBG wavefunctions. We also show that the Berry curvature distribution in these models can be continuously tuned while maintaining perfect quantum geometry. Similar to the study of fractional Chern insulators in ideal $C = 1$ bands, these models pave the way for investigating exotic topological phases in higher Chern bands for which no Landau level analog is available.

Introduction— The discovery of superconductivity and strongly correlated phases of matter in twisted graphene-based systems [1–3] has gone hand in hand with an exploration of their unique electronic structure including topological aspects [4–12] emphasized by the discovery of intrinsic Chern insulating phases [13–15]. While Chern quantization is topological, band geometry controls other interaction driven phenomena, including topological mechanisms for superconductivity and fractional Chern insulators (FCIs) [16–23]. Band geometry is quantified by the Berry curvature and the Fubini-Study metric. It is of great interest to understand the interplay between band flatness, Chern number and geometry. Of particular interest are bands with higher Chern number, which have no direct Landau level analog but can be realized in twisted graphene structures [24–29] without magnetic field, unlike Hofstadter systems [30–32].

The bands of twisted bilayer graphene, described by the Bistritzer-MacDonald (BM) model [4], are greatly simplified in the "chiral" model introduced by Tarnopolsky *et al.* [33] where the same-sublattice moiré tunneling vanishes. The chiral model has been extremely useful in understanding the physics of the system [34] due to its remarkable properties: (i) perfectly flat bands at a set of magic angles, (ii) explicitly obtainable wavefunctions that are equivalent to the wavefunctions of a Dirac particle in a magnetic field [18, 33], (iii) wavefunctions that satisfy the "trace condition" which relates the quantum metric to the Berry curvature; this allows the construction of Laughlin-like FCIs for short-range potentials [18, 22]. If a band satisfies (iii) we say that it has *ideal* quantum geometry. The chiral model has served as a useful starting point in numerical studies of FCIs [19–21]. Furthermore, it has inspired an improved understanding

of ideal $|C| = 1$ bands [22] and ideal Chern bands more broadly [35–41].

In this work we describe the first ideal higher Chern bands that are not fine-tuned [42–44] or combinations of $C = 1$ bands such as the lowest Landau level (LLL) [45]. Our models are continuum models of actively explored experimental systems without magnetic field and are not fine-tuned — their properties do not rely on specific relationships between parameters; instead we turn off subleading terms in the realistic Hamiltonians. We study a class of chiral models of n chirally-stacked graphene layers, e.g. AB, ABC, etc, where each successive pair of layers has the same Bernal stacking AB or BA, twisted on top of m chirally-stacked graphene layers [68]. Many of these structures are actively explored experimentally including twisted mono-bilayer graphene, $(n, m) = (2, 1)$ [26–28, 46] and twisted double bilayer $(n, m) = (2, 2)$ in both AB-AB stacking [47–51] and AB-BA stacking [29]. The flat bands and their Chern numbers have been studied [50, 52–56] and anomalous Hall states have been observed [24, 26–29]; it was noticed that these systems have similar magic angles to TBG [50, 52, 55]. However, the analytical nature of the wavefunctions and quantum geometry is thus far unknown.

We show that our models realize perfectly flat bands at the *same* magic angles as chiral TBG with ideal quantum geometry and Chern numbers $\pm n$ and $\mp m$ or ± 1 and $\mp(n + m - 1)$, depending on the chirality of the stacking (e.g. AB vs BA). We also show that the ideal geometry of these models is *intrinsically* $|C| > 1$; there is no decomposition into $|C|$ orthogonal ideal Chern ± 1 bands. We do this by identifying a general criterion for this splittability for $C = 2$ bands. Thus, our models go beyond previous idealized models of higher Chern number bands
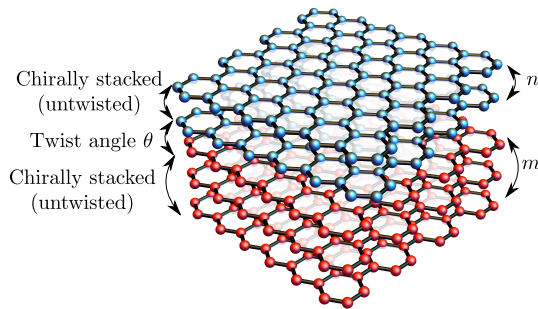
FIG. 1: Schematic illustration of our multilayer setting with n chirally stacked layers, e.g. AB, ABC, etc, such that each successive layers have the same Bernal stacking AB or BA, shown in blue with a twist angle θ on top of m chirally stacked layers (shown in red).

consisting of $|C|$ LLLs [45] while still maintaining ideal quantum geometry.

The ideal quantum geometry of these bands makes them especially suitable for realizing FCIs; we show that ideal quantum geometry enables the construction of FCI ground states through real-space holomorphicity. The ensuing realization of FCIs in higher Chern number bands would be remarkable, especially since defects in such systems, dubbed "genons", have non-Abelian statistics [57, 58]. Unlike chiral TBG, these models allow for arbitrarily inhomogeneous Berry curvature which will enable future studies to pinpoint the influence of inhomogeneous Berry curvature on the stability of FCI states.

Model— We consider the Hamiltonian for a single graphene valley

$$\mathcal{H} = \begin{pmatrix} h_{n,\sigma} & T_M \\ T_M^\dagger & h_{m,\sigma'} \end{pmatrix} \qquad (1)$$

where T_M is the chiral moiré tunneling which couples the n and $n + 1$ layers; it is zero except for $\alpha \begin{pmatrix} 0 & U(\boldsymbol{r}) \\ U^*(-\boldsymbol{r}) & 0 \end{pmatrix}$ in its lower left 2×2 block. Here, $U(\boldsymbol{r}) = \sum_{n=1}^{3} e^{\frac{2\pi i}{3}(n-1)} e^{-i\boldsymbol{q}_n \cdot \boldsymbol{r}}$ with $\boldsymbol{q}_n = 2k_D \sin\left(\frac{\theta}{2}\right) R_{\frac{2\pi(n-1)}{3}}(0,-1)$, $k_D = \frac{4\pi}{3\sqrt{3}a_{CC}}$, and $\alpha = \frac{w}{2\hbar v_F k_D \sin(\theta/2)}$ with w the opposite sublattice Moire tunneling. All energies are measured in units of $2\hbar v_F k_D \sin\frac{\theta}{2} = \frac{w}{\alpha}$.

The Hamiltonian $h_{n,\sigma}$, with $\sigma = \pm$, takes the form of $n \times n$ block diagonal matrix (with each block having a 2×2 structure in sublattice space) given explicitly by

$$h_{n,\pm} = \begin{pmatrix} -i\boldsymbol{\sigma} \cdot \nabla & T_\pm & 0 & \cdots \\ T_\pm^\dagger & -i\boldsymbol{\sigma} \cdot \nabla & T_\pm & \cdots \\ 0 & T_\pm^\dagger & -i\boldsymbol{\sigma} \cdot \nabla & \cdots \\ \cdots & \cdots & \cdots & \ddots \end{pmatrix}, \quad (2)$$

where $T_\pm = \beta \frac{\sigma_x \pm i\sigma_y}{2}$, with $\sigma_{x,y,z}$ denoting the Pauli ma-

trices in sublattice space, and $\beta = \frac{\gamma}{2\hbar v_F k_D \sin\frac{\theta}{2}}$, where γ is the interlayer tunneling of Bernal-stacked graphene. For realistic systems $w \approx 110$ meV, $\gamma \approx 360$ meV. The first magic angle occurs for $\alpha = 0.586$ at which $\beta \approx 1.9$.

The models (1) all have a moiré translation symmetry with lattice vectors $\boldsymbol{a}_{1,2} = \frac{4\pi}{3}(\pm\sqrt{3}/2, 1/2)$. It is useful to define an analogue of the magnetic length $2\pi\ell^2 = A$ where A is the unit cell area. The wavefunctions in layer l have the Bloch periodicity [33, 34] $\psi_{l,\boldsymbol{k}}(\boldsymbol{r} + \boldsymbol{a}_{1,2}) = e^{i(\boldsymbol{k}-\boldsymbol{K}_l)\cdot\boldsymbol{a}_{1,2}}\psi_{l,\boldsymbol{k}}(\boldsymbol{r})$, where $\boldsymbol{K} = -\boldsymbol{q}_1$ for $l \leq n$ and $\boldsymbol{K}' = \boldsymbol{q}_1$ for $l > n$ and $\boldsymbol{k} = 0$ corresponds to the Γ point. To incorporate these boundary conditions, we write $\psi_{l,\boldsymbol{k}}(\boldsymbol{r}) = e^{i(\boldsymbol{k}-\boldsymbol{K}_l)\cdot\boldsymbol{r}}u_{l,\boldsymbol{k}}(\boldsymbol{r})$, where $u_{l,\boldsymbol{k}}(\boldsymbol{r})$ is periodic in $\boldsymbol{r}$.

The Hamiltonian (1) is off-diagonal in the sublattice basis, $\{\mathcal{H}, \sigma_z\} = 0$, and so it may be written as

$$\mathcal{H} = \begin{pmatrix} 0 & \mathcal{D}^\dagger \\ \mathcal{D} & 0 \end{pmatrix}_{AB}. \qquad (3)$$

The ideal Chern bands will arise as zero modes of $\mathcal{H}$. They may be chosen to be sublattice polarized and thus zero modes of $\mathcal{D}, \mathcal{D}^\dagger$. Note that the equation $\mathcal{D}\psi = 0$ is equivalent to $\tilde{\mathcal{D}}u = 0$ where $\tilde{\mathcal{D}}$ is obtained from $\mathcal{D}$ by replacing the l-th diagonal entry by $-2i\bar{\partial} + k - K_l$ where we use the non-bold letter k to denote $k_x + ik_y$. We will use this notation for other vectors as well. Because $\tilde{\mathcal{D}}$ only depends on k and not $\bar{k}$ we may always choose u_k that are zero modes of $\tilde{D}$ to be holomorphic functions of k as well [18, 34].

Band Geometry — Here we say that the quantum geometry of a band is *ideal* if the band satisfies the trace condition. Without loss of generality we take $C > 0$; complex conjugation may be applied to obtain analogous statements for $C < 0$. The trace condition is the saturation of the inequality

$$\text{tr}g(\boldsymbol{k}) \geq \Omega(\boldsymbol{k}) \qquad (4)$$

where g is the Fubini-Study metric and Ω is the Berry curvature. The trace condition is necessary for reproducing LLL physics [18, 22, 34, 42, 59, 60] and it holds if and only if the wavefunctions $u_{\boldsymbol{k}}$ are holomorphic functions of $k_x + ik_y$ [22, 35]. If the trace condition holds and the Berry curvature is homogeneous then the density operators satisfy the Girvin-Macdonald-Platzmann algebra [61] of the LLL [59, 60].

We now show that the trace condition enables the construction of model fractional quantum Hall wavefunctions. The trace condition implies that $z\psi = Pz\psi$ for $z = x + iy$ and $P = \sum_{\boldsymbol{k}} |\psi_{\boldsymbol{k}}\rangle \langle\psi_{\boldsymbol{k}}|$ the projector onto the band of interest [41, 59]. Through iteration and power series we have $f(z)\psi = Pf(z)\psi$; multiplication by holomorphic functions does not take the wavefunction out of the band of interest. For many-body wavefunctions, we may then attach factors such as $\prod_{i<j}(z_i - z_j)^n$ without involving remote bands resulting in FCI ground states in

flat bands with short range interactions [18, 34, 62, 63]. So far, this conclusion has only been derived for the case of ideal $C = 1$ bands where the wavefunctions are related to LLL wavefunctions [22]. Our models allow for the extension of these ideas to higher Chern bands.

While the trace condition is sufficient to guarantee an FCI ground state in the limit of short ranged interactions, this limit may be difficult to reach when the Berry curvature is inhomogeneous. In the extreme limit of soleinoidal Berry curvature the band can energetically resemble a band of different Chern number [64]; this is easiest to see in a finite-size system where a concentrated Berry curvature is invisible to the momentum space grid. For the models we study, the Berry curvature may be tuned to be as inhomogeneous as one wishes, enabling future works to isolate the effect of inhomogenous Berry curvature while preserving the trace condition.

The Foundation: A Review of CMATBG— The foundation of the solution to the general multilayer models is $n = m = 1$, or CMATBG. Here we review the wavefunctions of CMATBG on the A sublattice [18, 33] that form a band of zero modes of the operator

$$\mathcal{D} = \begin{pmatrix} -2i\bar{\partial} & \alpha U(\boldsymbol{r}) \\ \alpha U(-\boldsymbol{r}) & -2i\bar{\partial} \end{pmatrix}. \qquad (5)$$

The B sublattice wavefunctions are related by $C_2 \mathcal{T}$: $\psi(\boldsymbol{r}) \mapsto \overline{\psi(-\boldsymbol{r})}$.

We will write u_k in terms of the (modified [65]) Weierstrass sigma function [22, 66] $\sigma(z) = \sigma(z|a_1, a_2)$ which satsfies $\sigma(z) = -\sigma(-z)$ and $\sigma(z + a_{1,2}) = -\exp\left(-\frac{1}{2\ell^2} a_{1,2}^*(z + \frac{a_{1,2}}{2})\right)\sigma(z)$. Together these imply $\sigma(a) = 0$ for all lattice vectors $\boldsymbol{a}$.

The function $\phi_k(\boldsymbol{r}) = e^{-\frac{i}{2} z^* k} \sigma(z + i\ell^2 k)$ satisfies $\phi_{\boldsymbol{k}+\boldsymbol{b}_i}(\boldsymbol{r}) = e^{-i\boldsymbol{b}_i \cdot \boldsymbol{r}} e^{i\theta_{k,b_i}} \phi_k(\boldsymbol{r})$ with $\theta_{k,b} = \pi - \frac{1}{2} i\ell^2 b^*(k - b/2)$ and is a building block for all the models in this paper.

The chiral TBG periodic wavefunction may be written as

$$u_k(\boldsymbol{r}) = \phi_{\boldsymbol{k}}(\boldsymbol{r}) \frac{u_\Gamma(\boldsymbol{r})}{\sigma(z)} = \phi_{\boldsymbol{k}}(\boldsymbol{r}) e^{-K(\boldsymbol{r})} \boldsymbol{n}(\boldsymbol{r}). \qquad (6)$$

Without the normalized layer spinor $\boldsymbol{n}(\boldsymbol{r})$, this wavefunction is that of a Dirac particle moving in an inhomogeneous magnetic field $B(\boldsymbol{r}) = \nabla^2 K(\boldsymbol{r})$ with one flux quantum per unit cell [18]. The spinor drops out of Bloch overlaps and therefore does not influence the quantum geometry of the system or the interacting physics for density-density interactions.

Throughout this paper we consider wavefunctions that are smooth in k but not periodic; one may always choose such a gauge. The Chern number may then be computed by taking the line integral of the Berry connection around the Brillouin zone and using the $\boldsymbol{k}$-space boundary conditions. One obtains [22, 34]

$$C = \frac{1}{2\pi} \operatorname{Re}(\theta_{k+b_1,b_2} - \theta_{k,b_2} + \theta_{k,b_1} - \theta_{k+b_2,b_1}). \qquad (7)$$

For CMATBG we see that $C = 1$.

Simple example: chiral twisted mono-bilayer graphene— We now show that the Hamiltonian (1) has perfectly flat bands at the same set of magic angles as chiral TBG. We start with $n = 2$, $m = 1$ and $\sigma = +$ corresponding to chiral twisted mono-bilayer. The zero mode operator is

$$\mathcal{D}(\boldsymbol{r}) = \begin{pmatrix} -2i\bar{\partial} & \beta & 0 \\ 0 & -2i\bar{\partial} & \alpha U(\boldsymbol{r}) \\ 0 & \alpha U(-\boldsymbol{r}) & -2i\bar{\partial} \end{pmatrix}. \qquad (8)$$

Let us start with sublattice A. The equations from the second and third rows of $\mathcal{D}\psi = 0$ are identical to those of CMATBG (5). Thus , we can write a solution to $\mathcal{D}\psi = 0$ with $\psi = (\psi_1, \psi_2, \psi_3)$ as follows:

$$\psi_{2,\boldsymbol{k}} = \lambda_{\boldsymbol{k}} \psi_{1,\boldsymbol{k}}^{\mathrm{TBG}}, \quad \psi_{3,\boldsymbol{k}} = \lambda_{\boldsymbol{k}} \psi_{2,\boldsymbol{k}}^{\mathrm{TBG}}, \quad 2i\bar{\partial}\psi_{1,\boldsymbol{k}} = \beta \lambda_{\boldsymbol{k}} \psi_{1,\boldsymbol{k}}^{\mathrm{TBG}} \qquad (9)$$

where $\lambda_{\boldsymbol{k}}$ is a $\boldsymbol{k}$-dependent constant to be determined soon.

In Fourier space, $u_{\boldsymbol{k}}(\boldsymbol{r}) = \sum_{\boldsymbol{G}} e^{i\boldsymbol{G}\cdot\boldsymbol{r}} u_{\boldsymbol{k}}(\boldsymbol{G})$, the last equation may be solved:

$$u_{1,\boldsymbol{k}}(\boldsymbol{G}) = -\frac{\beta \lambda_{\boldsymbol{k}}}{k - K + G} u_{1,\boldsymbol{k}}^{\mathrm{TBG}}(\boldsymbol{G}), \qquad (10)$$

$$u_{2,\boldsymbol{k}}(\boldsymbol{G}) = \lambda_{\boldsymbol{k}} u_{1,\boldsymbol{k}}^{\mathrm{TBG}}(\boldsymbol{G}), \quad u_{3,\boldsymbol{k}}(\boldsymbol{G}) = \lambda_{\boldsymbol{k}} u_{2,\boldsymbol{k}}^{\mathrm{TBG}}(\boldsymbol{G}). \qquad (11)$$

As discussed above, because (11) gives a band of zero modes of the operator $\tilde{\mathcal{D}}$ we may choose $u_{\boldsymbol{k}}$ and $\lambda_{\boldsymbol{k}}$ to only depend on k such that the band satisfies (4).

We now describe λ_k and obtain the Chern number. In order for (11) to be normalizable, we need λ_k to have a single zero at $k = K - G$ and no others. This fixes $\lambda_k = \phi_{k-K}(0)$ up to gauge transformations. Since the phase of $\lambda_{\boldsymbol{k}}$ winds by 2π around the BZ, multiplication by $\lambda_{\boldsymbol{k}}$ increases the Chern number by 1 compared to CMATBG. We may also compute the Chern number from the boundary condition method (7) and obtain 2 as well.

Let us now consider the B sublattice. Writing the operator $\mathcal{D}^\dagger$ explicitly

$$\mathcal{D}^\dagger = \begin{pmatrix} -2i\partial & 0 & 0 \\ \beta & -2i\partial & \alpha U^*(-\boldsymbol{r}) \\ 0 & \alpha U^*(\boldsymbol{r}) & -2i\partial \end{pmatrix} \qquad (12)$$

There is a zero energy state given by $\psi_B = (0, \psi_{B,1}^{\mathrm{TBG}}, \psi_{B,2}^{\mathrm{TBG}})$. Thus, we reproduce the B sublattice wavefunctions of CMATBG and obtain $C = -1$. Our result of two flat bands per valley with Chern numbers ± 2 and ∓ 1 is compatible with realistic twisted mono-bilayer graphene [28].

The previous analysis implies that the Hamiltonian (8) has the same magic angles as TBG: remarkably the angles are independent of the interlayer coupling β. This is illustrated in Fig. 2a-c, which shows the band structure at the first magic angle for different values of β. Although the bands remain flat, the overall band structure and flat
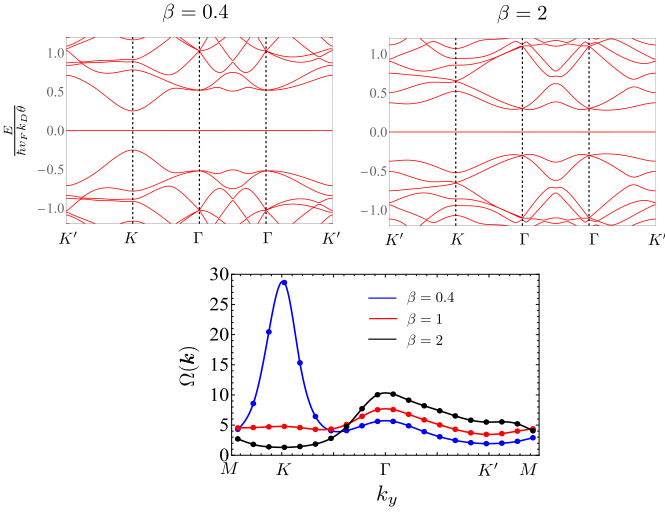
FIG. 2: **Band structure and Berry curvature for chiral twisted mono-bilayer graphene**: Band structure for the Hamiltonian (8) at the first magic angle for $\beta = 0.4, 2$ (top panel) and Berry curvature of the $C = 2$ band for $\beta = 0.4, 1, 2$ (bottom panel). For small β, the Berry curvature is strongly peaked at the K point and by increasing β, it gets more uniform with the peak moving to the Γ point. It is easy to check numerically that the trace condition $\mathrm{tr}\, g(\boldsymbol{k}) = |\Omega(\boldsymbol{k})|$ is always satisfied.

band wavefunctions depend on the parameter β. As $\beta \to 0$ the band gap closes and the Berry curvature diverges, as shown in Fig. 2e-g and the system decouples into $C = \pm 1$ chiral MATBG and graphene.

No decomposition into two ideal $C = 1$ bands— We now show that upon doubling the unit cell with translation breaking wavevector $\boldsymbol{Q}$, an ideal $C = 2$ band can be decomposed into two ideal orthogonal $C = 1$ bands if and only if the Berry curvature satisfies $\Omega(\boldsymbol{k}) = \Omega(\boldsymbol{k} + \boldsymbol{Q})$. Mono-bi graphene does not satisfy this condition.

We assume, and soon contradict, that the wavefunctions of the two $C = 1$ bands $|\tilde{u}_{k\zeta}\rangle$ for $\zeta = 1, 2$ are holomorphic in k and therefore may be written as $|\tilde{u}_{\zeta k}\rangle = \alpha_{\zeta k} |u_k\rangle + \beta_{\zeta k} e^{i\boldsymbol{Q}\cdot\boldsymbol{r}} |u_{k+Q}\rangle$ for some holomorphic $\alpha_{\zeta k}$ and $\beta_{\zeta k}$. The orthogonality $\langle \tilde{u}_{k2} | \tilde{u}_{k1} \rangle = 0$ implies $-\frac{\beta_{k1}\overline{\beta_{k2}}}{\alpha_{k1}\overline{\alpha_{k2}}} = \frac{\|u_k\|^2}{\|u_{k+Q}\|^2}$, where we used $\langle u_k | e^{i\boldsymbol{Q}\cdot\boldsymbol{r}} | u_{k+Q}\rangle = 0$ and we work in a patch of k space away from zeros of α_ζ. The right hand side is positive; thus we have $\frac{\beta_{2k}}{\alpha_{2k}} = -c\frac{\beta_{1k}}{\alpha_{1k}}$ for a real positive c. Let us define $e^{w_k} = \beta_{1k}/\alpha_{1k}$; then we have $\mathrm{Re}\, w_k = \log \frac{c\|u_k\|}{\|u_{k+Q}\|}$. Real parts of holomorphic functions are harmonic (have zero laplacian), and a holomorphic function may be reconstructed from a harmonic real part. Therefore the decomposition is possible and unique if and only if $\nabla^2 \log \frac{\|u_k\|}{\|u_{k+Q}\|} = \Omega(\boldsymbol{k}) - \Omega(\boldsymbol{k}+\boldsymbol{Q}) = 0$ for all $\boldsymbol{k}$; here we used $\Omega(\boldsymbol{k}) = \nabla^2 \log \|u_k\|$ [22, 39].

General case— We now generalize to arbitrary n, m,

(σ, σ')	Chern A	Chern B
$(+, +)$	n	$-m$
$(-, +)$	1	$-(n + m - 1)$
$(+, -)$	$n + m - 1$	-1
$(-, -)$	m	$-n$

TABLE I: Chern numbers for the A and B sublattice bands for a configuration of n-layers twisted on top of m-layers.

σ and σ'. It is sufficient to focus on sublattice A and $(\sigma, \sigma') = (+, +), (+, -)$ and $(-, +)$. Any sublattice B band may be mapped to a sublattice A band using $C_{2z}\mathcal{T}$, under which valley is kept invariant, sublattices are exchanged, Chern number switches sign and layers are kept invariant: $(n, m, \sigma, \sigma') \mapsto (n, m, -\sigma, -\sigma')$. Next, we may map $(-, -) \to (+, +)$ stacking by $C_{2y}\mathcal{T}$ under which the valley, sublattice, and Chern number are kept invariant while $l \mapsto n + m - l + 1$ which switches chirality: $(n, m, \sigma, \sigma') \mapsto (m, n, -\sigma', -\sigma)$.

We first consider $(\sigma, \sigma') = (+, -)$. As before $\psi_n = \lambda_{\boldsymbol{k}} \psi_1^{\mathrm{TBG}}$ and $\psi_{n+1} = \lambda_{\boldsymbol{k}} \psi_2^{\mathrm{TBG}}$. The remaining components are given by solving the equations $2i\bar{\partial}\psi_l = \beta\psi_{l+1}$ for $l < n$ and $2i\bar{\partial}\psi_l = \beta\psi_{l-1}$ for $l > n + 1$. These equations have the solution

$$u_{l,\boldsymbol{k}}(\boldsymbol{G}) = \lambda_{\boldsymbol{k}} \left(\frac{-\beta}{k - K + G} \right)^{n-l} u_{1,\boldsymbol{k}}^{\mathrm{TBG}}(\boldsymbol{G}), \quad l \leq n \quad (13)$$

$$u_{l,\boldsymbol{k}}(\boldsymbol{G}) = \lambda_{\boldsymbol{k}} \left(\frac{-\beta}{k - K' + G} \right)^{m-(l-n)} u_{2,\boldsymbol{k}}^{\mathrm{TBG}}(\boldsymbol{G}), \quad l > n \tag{14}$$

This yields a normalizable wavefunction if and only if λ_k has a zero of order $n - 1$ whenever $\boldsymbol{k} = \boldsymbol{K} - \boldsymbol{G}$, a zero of order $m - 1$ whenever $\boldsymbol{k} = \boldsymbol{K}' - \boldsymbol{G}$, and no others which gives a total Chern number of $n + m - 1$. We have $\lambda_k = \phi_{k-K}(0)^{n-1}\phi_{k-K'}(0)^{m-1}$. For $l < n$, the wavefunction $u_{lk}(\boldsymbol{r})$ contains the factor $\phi_{k-K}(0)^{l-1}\phi_{k-K'}(0)^{m-1}$, as well as $m - 1$ zeros at $k = K'$. Analogous considerations apply to the case $l > n$.

For $(\sigma, \sigma') = (+, +)$ we may set $u_{kl} = 0$ for $l > n + 1$. The $l \leq n$ wavefunctions are then the same as the $(\sigma, \sigma') = (+, -)$ case with $m = 1$. Finally, for $(\sigma, \sigma') = (-, +)$ we recover chiral TBG wavefunctions. A summary of the results is provided in Table I. The wavefunctions u_k are always analytic in k which means that the bands always have ideal quantum geometry.

Berry curvature variations— The models introduced here provide a realization of ideal higher Chern bands where the Berry curvature is continuously tunable and arbitrarily inhomogeneous. This is illustrated in Fig. 3 by plotting the Berry deviation

$$F = \left(\int \frac{d^2\boldsymbol{k}}{A_{\mathrm{BZ}}} \left[\frac{A_{\mathrm{BZ}}\Omega(\boldsymbol{k})}{2\pi C} - 1 \right]^2 \right)^{1/2} \tag{15}$$
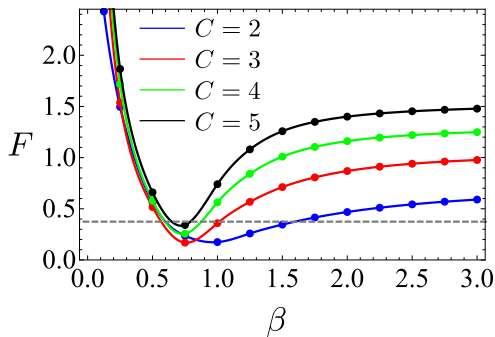
FIG. 3: **Berry deviations:** Plot of the Berry inhomogeneity F defined in Eq. 15 as a function of β for $C = 2, 3, 4, 5$ obtained from models with $n = 2, 3, 4, 5$ and $m = 1$. The dashed line indicates the corresponding value of $C = 1$ CMATBG bands.

for bands with $C = 2, 3, 4, 5$ as a function of the Bernal-stack coupling parameter β. As we can see, F diverges in the decoupled $\beta \to 0$ limit. The minimal value of F occurs around $\beta \approx 0.75 - 1$, and for the realistic $\beta \approx 1.9$ the inhomogeneity is not very large.

Conclusion Here we have shown that a family of chirally twisted graphene structures can, in a particular limit, realize flat and ideal Chern bands with arbitrary Chern numbers. This setup has a new tuning parameter which strongly affects Berry curvature distribution while keeping the ideal quantum band geometry intact despite having the same magic angle as twisted bilayer graphene. Although the ideal limit discussed here is not perfectly realized in actual materials, additional terms like a displacement field may help access this limit in realistic systems. Independent of their realizability, our models are a promising starting point for exploring exotic topological phases at fractional filling of ideal flat higher Chern bands whose interaction physics is poorly understood due to the lack a Landau level analog.

Note Added During the completion of this work, Ref [67] appeared, which overlaps with the results reported here.

[1] Yuan Cao, Valla Fatemi, Shiang Fang, Kenji Watanabe, Takashi Taniguchi, Efthimios Kaxiras, and Pablo Jarillo-Herrero. Unconventional superconductivity in magic-angle graphene superlattices. *Nature*, 556(7699):43–50, Apr 2018.

[2] Yuan Cao, Valla Fatemi, Ahmet Demir, Shiang Fang, Spencer L. Tomarken, Jason Y. Luo, Javier D. Sanchez-Yamagishi, Kenji Watanabe, Takashi Taniguchi, Efthimios Kaxiras, Ray C. Ashoori, and Pablo Jarillo-Herrero. Correlated insulator behaviour at half-filling in magic-angle graphene superlattices. *Nature*, 556(7699):80–84, Apr 2018.

[3] Leon Balents, Cory R. Dean, Dmitri K. Efetov, and Andrea F. Young. Superconductivity and strong correlations in moiréflat bands. *Nature Physics*, 16(7):725–733, 2020.

[4] Rafi Bistritzer and Allan H. MacDonald. Moiré bands in twisted double-layer graphene. *Proceedings of the National Academy of Sciences*, 108(30):12233–12237, 2011.

[5] E Suárez Morell, JD Correa, P Vargas, M Pacheco, and Z Barticevic. Flat bands in slightly twisted bilayer graphene: Tight-binding calculations. *Physical Review B*, 82(12):121407, 2010.

[6] J. M. B. Lopes dos Santos, N. M. R. Peres, and A. H. Castro Neto. Continuum model of the twisted graphene bilayer. *Phys. Rev. B*, 86:155449, Oct 2012.

[7] Hoi Chun Po, Liujun Zou, Ashvin Vishwanath, and T. Senthil. Origin of mott insulating behavior and superconductivity in twisted bilayer graphene. *Phys. Rev. X*, 8:031089, Sep 2018.

[8] Hoi Chun Po, Liujun Zou, T. Senthil, and Ashvin Vishwanath. Faithful tight-binding models and fragile topology of magic-angle bilayer graphene. *Physical Review B*, 99(19), May 2019.

[9] Eslam Khalaf, Alex J. Kruchkov, Grigory Tarnopolsky, and Ashvin Vishwanath. Magic angle hierarchy in twisted graphene multilayers. *Phys. Rev. B*, 100:085109, Aug 2019.

[10] Junyeong Ahn, Sungjoon Park, and Bohm-Jung Yang. Failure of Nielsen-Ninomiya Theorem and Fragile Topology in Two-Dimensional Systems with Space-Time Inversion Symmetry: Application to Twisted Bilayer Graphene at Magic Angle. *Physical Review X*, 9(2):021013, Apr 2019.

[11] Zhida Song, Zhijun Wang, Wujun Shi, Gang Li, Chen Fang, and B. Andrei Bernevig. All magic angles in twisted bilayer graphene are topological. *Phys. Rev. Lett.*, 123:036401, Jul 2019.

[12] Ya-Hui Zhang, Dan Mao, and T. Senthil. Twisted bilayer graphene aligned with hexagonal boron nitride: Anomalous hall effect and a lattice model. *Phys. Rev. Research*, 1:033126, Nov 2019.

[13] Aaron L. Sharpe, Eli J. Fox, Arthur W. Barnard, Joe Finney, Kenji Watanabe, Takashi Taniguchi, M. A. Kastner, and David Goldhaber-Gordon. Emergent ferromagnetism near three-quarters filling in twisted bilayer graphene. *Science*, 365(6453):605–608, 2019.

[14] M. Serlin, C. L. Tschirhart, H. Polshyn, Y. Zhang, J. Zhu, K. Watanabe, T. Taniguchi, L. Balents, and A. F. Young. Intrinsic quantized anomalous hall effect in a moiré heterostructure. *Science*, 367(6480):900–903, 2020.

[15] Eva Y. Andrei and Allan H. MacDonald. Graphene bi-

layers with a twist. *Nature Materials*, 19(12):1265–1275, 2020.

[16] Eslam Khalaf, Shubhayu Chatterjee, Nick Bultinck, Michael P. Zaletel, and Ashvin Vishwanath. Charged skyrmions and topological origin of superconductivity in magic-angle graphene. *Science Advances*, 7(19), 2021.

[17] Shubhayu Chatterjee, Matteo Ippoliti, and Michael P. Zaletel. Skyrmion superconductivity: DMRG evidence for a topological route to superconductivity. *arXiv preprint arXiv:2010.01144*, 2020.

[18] Patrick J. Ledwith, Grigory Tarnopolsky, Eslam Khalaf, and Ashvin Vishwanath. Fractional chern insulator states in twisted bilayer graphene: An analytical approach. *Phys. Rev. Research*, 2:023237, May 2020.

[19] Cécile Repellin, Zhihuan Dong, Ya-Hui Zhang, and T. Senthil. Ferromagnetism in narrow bands of moiré superlattices. *Phys. Rev. Lett.*, 124:187601, May 2020.

[20] Patrick Wilhelm, Thomas C. Lang, and Andreas M. Läuchli. Interplay of fractional chern insulator and charge density wave phases in twisted bilayer graphene. *Phys. Rev. B*, 103:125406, Mar 2021.

[21] Ahmed Abouelkomsan, Zhao Liu, and Emil J. Bergholtz. Particle-hole duality, emergent fermi liquids, and fractional chern insulators in moiré flatbands. *Phys. Rev. Lett.*, 124:106803, Mar 2020.

[22] Jie Wang, Jennifer Cano, Andrew J. Millis, Zhao Liu, and Bo Yang. Exact landau level description of geometry and interaction in a flatband. *Phys. Rev. Lett.*, 127:246403, Dec 2021.

[23] Yonglong Xie, Andrew T. Pierce, Jeong Min Park, Daniel E. Parker, Eslam Khalaf, Patrick Ledwith, Yuan Cao, Seung Hwan Lee, Shaowen Chen, Patrick R. Forrester, Kenji Watanabe, Takashi Taniguchi, Ashvin Vishwanath, Pablo Jarillo-Herrero, and Amir Yacoby. Fractional chern insulators in magic-angle twisted bilayer graphene. *Nature*, 600(7889):439–443, Dec 2021.

[24] Xiaomeng Liu, Zeyu Hao, Eslam Khalaf, Jong Yeon Lee, Yuval Ronen, Hyobin Yoo, Danial Haei Najafabadi, Kenji Watanabe, Takashi Taniguchi, Ashvin Vishwanath, and et al. Tunable spin-polarized correlated states in twisted double bilayer graphene. *Nature*, 583(7815):221225, Jul 2020.

[25] Yuan Cao, Daniel Rodan-Legrain, Oriol Rubies-Bigorda, Jeong Min Park, Kenji Watanabe, Takashi Taniguchi, and Pablo Jarillo-Herrero. Tunable correlated states and spin-polarized phases in twisted bilayerbilayer graphene. *Nature*, 583(7815):215220, May 2020.

[26] Shaowen Chen, Minhao He, Ya-Hui Zhang, Valerie Hsieh, Zaiyao Fei, K. Watanabe, T. Taniguchi, David H. Cobden, Xiaodong Xu, Cory R. Dean, and Matthew Yankowitz. Electrically tunable correlated and topological states in twisted monolayer–bilayer graphene. *Nature Physics*, 17(3):374–380, Mar 2021.

[27] Minhao He, Ya-Hui Zhang, Yuhao Li, Zaiyao Fei, Kenji Watanabe, Takashi Taniguchi, Xiaodong Xu, and Matthew Yankowitz. Competing correlated states and abundant orbital magnetism in twisted monolayer-bilayer graphene. *Nature Communications*, 12(1):4727, Aug 2021.

[28] H. Polshyn, Y. Zhang, M. A. Kumar, T. Soejima, P. Ledwith, K. Watanabe, T. Taniguchi, A. Vishwanath, M. P. Zaletel, and A. F. Young. Topological charge density waves at half-integer filling of a moiré superlattice. *Nature Physics*, Dec 2021.

[29] Minhao He, Jiaqi Cai, Ya-Hui Zhang, Yang Liu, Yuhao Li, Takashi Taniguchi, Kenji Watanabe, David H. Cobden, Matthew Yankowitz, and Xiaodong Xu. Chirality-dependent topological states in twisted double bilayer graphene, 2021.

[30] Gunnar Möller and Nigel R. Cooper. Fractional chern insulators in harper-hofstadter bands with higher chern number. *Phys. Rev. Lett.*, 115:126401, Sep 2015.

[31] Bartholomew Andrews and Gunnar Möller. Stability of fractional chern insulators in the effective continuum limit of harper-hofstadter bands with chern number $|c| > 1$. *Phys. Rev. B*, 97:035159, Jan 2018.

[32] Bartholomew Andrews, Titus Neupert, and Gunnar Möller. Stability, phase transitions, and numerical breakdown of fractional chern insulators in higher chern bands of the hofstadter model. *Phys. Rev. B*, 104:125107, Sep 2021.

[33] Grigory Tarnopolsky, Alex Jura Kruchkov, and Ashvin Vishwanath. Origin of magic angles in twisted bilayer graphene. *Phys. Rev. Lett.*, 122:106405, Mar 2019.

[34] Patrick J. Ledwith, Eslam Khalaf, and Ashvin Vishwanath. Strong coupling theory of magic-angle graphene: A pedagogical introduction. *Annals of Physics*, 435:168646, 2021. Special issue on Philip W. Anderson.

[35] Bruno Mera and Tomoki Ozawa. Kähler geometry and chern insulators: Relations between topology and the quantum metric. *Phys. Rev. B*, 104:045104, Jul 2021.

[36] Tomoki Ozawa and Bruno Mera. Relations between topology and the quantum metric for chern insulators. *Phys. Rev. B*, 104:045103, Jul 2021.

[37] Anwei Zhang. Revealing chern number from quantum metric. *Chinese Physics B*, 2021.

[38] Bruno Mera, Anwei Zhang, and Nathan Goldman. Relating the topology of dirac hamiltonians to quantum geometry: When the quantum metric dictates chern numbers and winding numbers. *arXiv preprint arXiv:2106.00800*, 2021.

[39] Bruno Mera and Tomoki Ozawa. Engineering geometrically flat chern bands with fubini-study kähler structure. *Phys. Rev. B*, 104:115160, Sep 2021.

[40] Steven H. Simon and Mark S. Rudner. Contrasting lattice geometry dependent versus independent quantities: Ramifications for berry curvature, energy gaps, and dynamics. *Phys. Rev. B*, 102:165148, Oct 2020.

[41] Daniel Varjas, Ahmed Abouelkomsan, Kang Yang, and Emil J Bergholtz. Topological lattice models with constant berry curvature. *arXiv preprint arXiv:2107.06902*, 2021.

[42] Martin Claassen, Ching Hua Lee, Ronny Thomale, Xiao-Liang Qi, and Thomas P. Devereaux. Position-momentum duality and fractional quantum hall effect in chern insulators. *Phys. Rev. Lett.*, 114:236802, Jun 2015.

[43] Ching Hua Lee, Martin Claassen, and Ronny Thomale. Band structure engineering of ideal fractional chern insulators. *Phys. Rev. B*, 96:165150, Oct 2017.

[44] Jörg Behrmann, Zhao Liu, and Emil J. Bergholtz. Model fractional chern insulators. *Phys. Rev. Lett.*, 116:216802, May 2016.

[45] Yang-Le Wu, N. Regnault, and B. Andrei Bernevig. Bloch model wave functions and pseudopotentials for all fractional chern insulators. *Phys. Rev. Lett.*, 110:106802, Mar 2013.

[46] E. S. Morell, M. Pacheco, L. Chico, and L. Brey. Electronic properties of twisted trilayer graphene. *Physical*

Review B, 87:125414, 2013.

[47] Xiaomeng Liu, Zeyu Hao, Eslam Khalaf, Jong Yeon Lee, Yuval Ronen, Hyobin Yoo, Danial Haei Najafabadi, Kenji Watanabe, Takashi Taniguchi, Ashvin Vishwanath, and Philip Kim. Tunable spin-polarized correlated states in twisted double bilayer graphene. *Nature*, 583(7815):221–225, Jul 2020.

[48] Yuan Cao, Daniel Rodan-Legrain, Oriol Rubies-Bigorda, Jeong Min Park, Kenji Watanabe, Takashi Taniguchi, and Pablo Jarillo-Herrero. Tunable correlated states and spin-polarized phases in twisted bilayer–bilayer graphene. *Nature*, 583(7815):215–220, Jul 2020.

[49] Minhao He, Yuhao Li, Jiaqi Cai, Yang Liu, K. Watanabe, T. Taniguchi, Xiaodong Xu, and Matthew Yankowitz. Symmetry breaking in twisted double bilayer graphene. *Nature Physics*, 17(1):26–30, Jan 2021.

[50] Ya-Hui Zhang, Dan Mao, Yuan Cao, Pablo Jarillo-Herrero, and T. Senthil. Nearly flat chern bands in moiré superlattices. *Phys. Rev. B*, 99:075127, Feb 2019.

[51] Jong Yeon Lee, Eslam Khalaf, Shang Liu, Xiaomeng Liu, Zeyu Hao, Philip Kim, and Ashvin Vishwanath. Theory of correlated insulating behaviour and spin-triplet superconductivity in twisted double bilayer graphene. *Nature Communications*, 2019.

[52] Jianpeng Liu, Zhen Ma, Jinhua Gao, and Xi Dai. Quantum valley hall effect, orbital magnetism, and anomalous hall effect in twisted multilayer graphene systems. *Phys. Rev. X*, 9:031021, Aug 2019.

[53] Fatemeh Haddadi, QuanSheng Wu, Alex J. Kruchkov, and Oleg V. Yazyev. Moiré flat bands in twisted double bilayer graphene. *Nano Letters*, 20(4):2410–2415, Apr 2020.

[54] ShengNan Zhang, Bo Xie, QuanSheng Wu, Jianpeng Liu, and Oleg V Yazyev. Chiral decomposition of twisted graphene multilayers with arbitrary stacking. *arXiv preprint arXiv:2012.11964*, 2020.

[55] Zhen Ma, Shuai Li, Meng-Meng Xiao, Ya-Wen Zheng, Ming Lu, HaiWen Liu, Jin-Hua Gao, and XC Xie. Moir\'{e} flat bands of twisted few-layer graphite. *arXiv preprint arXiv:2001.07995*, 2020.

[56] Narasimha Raju Chebrolu, Bheema Lingam Chittari, and Jeil Jung. Flat bands in twisted double bilayer graphene. *Phys. Rev. B*, 99:235417, Jun 2019.

[57] Maissam Barkeshli and Xiao-Liang Qi. Topological nematic states and non-abelian lattice dislocations. *Phys. Rev. X*, 2:031013, Aug 2012.

[58] Maissam Barkeshli, Chao-Ming Jian, and Xiao-Liang Qi. Twist defects and projective non-abelian braiding statistics. *Phys. Rev. B*, 87:045130, Jan 2013.

[59] Rahul Roy. Band geometry of fractional topological insulators. *Phys. Rev. B*, 90:165139, Oct 2014.

[60] Siddharth A. Parameswaran, Rahul Roy, and Shivaji L. Sondhi. Fractional quantum hall physics in topological flat bands. *Comptes Rendus Physique*, 14(9):816 – 839, 2013. Topological insulators / Isolants topologiques.

[61] S. M. Girvin, A. H. MacDonald, and P. M. Platzman. Magneto-roton theory of collective excitations in the fractional quantum hall effect. *Phys. Rev. B*, 33:2481–2494, Feb 1986.

[62] F. D. M. Haldane. Fractional quantization of the hall effect: A hierarchy of incompressible quantum fluid states. *Phys. Rev. Lett.*, 51:605–608, Aug 1983.

[63] S. A. Trugman and S. Kivelson. Exact results for the fractional quantum hall effect with general interactions. *Phys. Rev. B*, 31:5280–5284, Apr 1985.

[64] Eslam Khalaf, Nick Bultinck, Ashvin Vishwanath, and Michael P Zaletel. Soft modes in magic angle twisted bilayer graphene. *arXiv preprint arXiv:2009.14827*, 2020.

[65] F. D. M. Haldane. A modular-invariant modified weierstrass sigma-function as a building block for lowest-landau-level wavefunctions on the torus. *Journal of Mathematical Physics*, 59(7):071901, 2018.

[66] Jie Wang, Yunqin Zheng, Andrew J. Millis, and Jennifer Cano. Chiral approximation to twisted bilayer graphene: Exact intravalley inversion symmetry, nodal structure, and implications for higher magic angles. *Phys. Rev. Research*, 3:023155, May 2021.

[67] Jie Wang and Zhao Liu. Hierarchy of ideal flatbands in chiral twisted multilayer graphene models. *arXiv preprint arXiv:2109.10325*, 2021.

[68] The word chiral is used in two distinct senses, the chiral stacking indicates the stacking pattern of graphene layers while the chiral model or limit refers to switching off same-sublattice moiré hoppings.